

Cite this: *RSC Adv.*, 2017, **7**, 30650

## Cathodic shift of a photo-potential on a $\text{Ta}_3\text{N}_5$ photoanode by post-heating a $\text{TiO}_2$ passivation layer†

Jie Liu,<sup>a</sup> Wenjun Luo,  <sup>\*a</sup> Kaijian Zhu,<sup>a</sup> Xin Wen,<sup>b</sup> Fei Xiu,<sup>a</sup> Jiajie Yuan,<sup>a</sup> Zhigang Zou<sup>b</sup> and Wei Huang<sup>\*ac</sup>

$\text{Ta}_3\text{N}_5$  is a promising photoanode material for solar water splitting due to its suitable band gap and high theoretical solar energy conversion. A high onset potential of  $\text{Ta}_3\text{N}_5$  limits its photoelectrochemical performance due to serious surface charge recombination. In a previous study, a  $\text{TiO}_2$  passivation layer was usually coated on the surface of  $\text{Ta}_3\text{N}_5$  to reduce the surface recombination and improve the performance of a sample. However, to date, there are no studies on the effect of conductivity of the  $\text{TiO}_2$  passivation layer on the photoelectrochemical properties of a  $\text{Ta}_3\text{N}_5$  photoanode. In this work, for the first time, the conductivity of  $\text{TiO}_2$  is increased by post-heating of a  $\text{TiO}_2$  passivation layer, leading to a 90 mV cathodic shift of the photo-potential of  $\text{Ta}_3\text{N}_5$ . After further loading with a  $\text{Ni(OH)}_x/\text{FeOOH}$  bilayer electrocatalyst, the  $\text{Ta}_3\text{N}_5$  photoanode achieves a current density of  $6.4 \text{ mA cm}^{-2}$  at  $1.23 \text{ V}_{\text{RHE}}$  and a HC-STH (half-cell solar to hydrogen efficiency) of 0.72% under a sunlight simulator ( $100 \text{ mW cm}^{-2}$ ), which are the highest values among the  $\text{Ta}_3\text{N}_5$  photoanodes prepared by thermal oxidation and nitridation of Ta foil.

Received 25th April 2017  
 Accepted 29th May 2017

DOI: 10.1039/c7ra04647b  
[rsc.li/rsc-advances](http://rsc.li/rsc-advances)

## 1. Introduction

Since Fujishima and Honda reported the use of a  $\text{TiO}_2$  photoanode to split water into  $\text{H}_2$  and  $\text{O}_2$  under illumination,<sup>1</sup> solar water splitting has become a promising method to convert solar energy into clean and high energy density  $\text{H}_2$ .<sup>2,3</sup> In the past forty years, three kinds of photoelectrochemical (PEC) cells, including PV (photovoltaic) + electrolysis, PV + PEC and a p-n tandem cell, have been explored.<sup>4-9</sup> In a p-n tandem cell, a n-type semiconductor as a photoanode is ohmically contacted with a p-type semiconductor as a photocathode. A two-photon system is used to split water in a p-n tandem cell and has higher efficiency than that of a conventional single-photon cell. Moreover, no expensive PV cells are used. Therefore, a p-n tandem cell is the most promising one due to its high theoretical efficiency and low cost.<sup>10,11</sup>

Recently, some n-type semiconductors,  $\text{BiVO}_4$ ,  $\text{Fe}_2\text{O}_3$  and  $\text{Ta}_3\text{N}_5$ , have been intensively studied as photoanodes.<sup>12-15</sup> The band gap of  $\text{BiVO}_4$  is too wide (2.4 eV), which leads to a low theoretical efficiency (9.1%), even lower than the minimum efficiency (10%) for practical applications.<sup>12</sup> Though  $\text{Fe}_2\text{O}_3$  has a high theoretical efficiency (16%), most of the samples achieve photocurrent lower than  $4 \text{ mA cm}^{-2}$ , which leads to an experimental efficiency lower than 5%.<sup>16,17</sup> The low efficiency is due to an intrinsic short hole diffusion length caused by a local d-band composition in valence band of  $\text{Fe}_2\text{O}_3$ .<sup>18</sup> In 2002,  $\text{Ta}_3\text{N}_5$  was firstly reported as a visible light photocatalyst for water splitting by Domen's group.<sup>19</sup> Though  $\text{Ta}_3\text{N}_5$  has a similar band gap (2.1 eV) and theoretical photocurrent with  $\text{Fe}_2\text{O}_3$ , a valence band of  $\text{Ta}_3\text{N}_5$  is composed of N2p and has a longer hole diffusion length than that of  $\text{Fe}_2\text{O}_3$ . Moreover, the bottom of conduction band of  $\text{Ta}_3\text{N}_5$  is at  $-0.3 \text{ V}_{\text{RHE}}$ , 0.6 V higher than that of  $\text{Fe}_2\text{O}_3$ , which means a more negative onset potential and a lower bias for photoelectrochemical water oxidation.<sup>20,21</sup> Therefore, it is easier for a  $\text{Ta}_3\text{N}_5$  photoanode to obtain high efficiency than  $\text{Fe}_2\text{O}_3$ . In recent years, photocurrent of  $\text{Ta}_3\text{N}_5$  has been boosted to a theoretical maximum value.<sup>14,22-24</sup> However, an onset potential of a  $\text{Ta}_3\text{N}_5$  photoanode ( $0.6-0.8 \text{ V}_{\text{RHE}}$ ) is still much positive than the theoretical value ( $-0.3 \text{ V}_{\text{RHE}}$ ) even after coating efficient electrocatalysts on the surface of  $\text{Ta}_3\text{N}_5$  to accelerate interface charge transfer.<sup>22,25-27</sup> The positive onset potential of a  $\text{Ta}_3\text{N}_5$  photoanode mainly originates from poor bulk transport of majority carriers and severe surface carrier recombination.<sup>14,28,29</sup> In order to further lower an onset potential, a  $\text{TiO}_2$

<sup>a</sup>Key Laboratory of Flexible Electronics (KLOFE), Institute of Advanced Materials (IAM), Jiangsu National Synergetic Innovation Center for Advanced Materials (SICAM), Nanjing Tech University (Nanjing Tech), 30 South Puzhu Road, Nanjing 211816, P. R. China. E-mail: iamwjluo@njtech.edu.cn; iamwhuang@njtech.edu.cn

<sup>b</sup>Eco-materials and Renewable Energy Research Center (ERERC), National Laboratory of Solid State Microstructures, Department of Physics, Nanjing University, Nanjing 210093, P. R. China

<sup>c</sup>Key Laboratory for Organic Electronics & Information Displays (KLOEID), Institute of Advanced Materials (IAM), Nanjing University of Posts and Telecommunications, Wenyuan Road 9, Nanjing 210023, China

† Electronic supplementary information (ESI) available. See DOI: [10.1039/c7ra04647b](https://doi.org/10.1039/c7ra04647b)



surface passivation layer was coated on the surface of  $\text{Ta}_3\text{N}_5$  because  $\text{TiO}_2$  could reduce surface recombination of photo-generated carriers.<sup>30–33</sup> However, to date, there are few studies on effect of conductivity of the  $\text{TiO}_2$  passivation layer on photoelectrochemical property of a  $\text{Ta}_3\text{N}_5$  photoanode.

In this study, we found that the large amount of  $\text{OH}^-$  group exist in an as-deposited  $\text{TiO}_2$  passivation layer to form  $\text{TiO}_x(\text{OH})_y$ , which impeded interface hole transfer and limited a conversion efficiency of  $\text{Ta}_3\text{N}_5$ . A strategy of post-heating of  $\text{TiO}_2$  passivation layer was proposed to cathodically shift photo-potential of  $\text{Ta}_3\text{N}_5$  by about 90 mV. After post-heating at a low temperature,  $\text{TiO}_x(\text{OH})_y$  in the as-deposited passivation layer was dehydrated into  $\text{TiO}_x(\text{OH})_{y-\delta}$ , which enhanced the interface hole transfer. Therefore, an onset potential of a  $\text{Ta}_3\text{N}_5$  photoanode was cathodically shifted. To the best of our knowledge, it is the first time to shift the onset potential of  $\text{Ta}_3\text{N}_5$  by heating a  $\text{TiO}_2$  passivation layer at a low temperature. This strategy not only deepens understanding the role of a  $\text{TiO}_2$  passivation layer in a photoelectrochemical cell but also offers reference to improve the performance of other photoelectrodes.

## 2. Experimental section

### 2.1 Preparation of $\text{Ta}_3\text{N}_5$ photoanodes

$\text{Ta}_3\text{N}_5$  photoanodes were prepared by modified oxidation and nitridation of Ta foils at a high temperature.<sup>14</sup> Ta foils ( $7 \times 16$  mm) were firstly rinsed by isopropanol, acetone and ethanol before use, respectively. In order to remove the oxygen-rich surface recombination layer, Ta foils were etched in 5 mL hydrofluoric acid solution (40%) for 225 min at room temperature (25 °C), and then rinsed with distilled water and ethanol. The etched Ta foils were calcined in air at 554 °C for 30 min to obtain  $\text{Ta}_2\text{O}_5$  film, followed by a further nitridation treatment under a flow of ammonia gas (800 mL min<sup>-1</sup>) at 900 °C for 8 h to become  $\text{Ta}_3\text{N}_5$ . A Ta foil without etching was also calcined in the same conditions as a reference to investigate the etching effect.

### 2.2 Deposition of a $\text{TiO}_2$ passivation layer

A  $\text{TiO}_2$  passivation layer was deposited by CBD method.<sup>24</sup> 200  $\mu\text{L}$  of titanium trichloride solution (20%) was added into 20 mL of deionized water in ice water bath. A  $\text{Ta}_3\text{N}_5$  sample was vertically immersed into the obtained solution, and a  $\text{TiO}_2$  passivation layer was deposited on the surface of a  $\text{Ta}_3\text{N}_5$  sample at 70 °C for 6 min. After washed with distilled water, the  $\text{TiO}_2$  coated  $\text{Ta}_3\text{N}_5$  electrode was calcined in nitrogen atmosphere at different temperatures (100 °C, 150 °C, 200 °C, and 250 °C) for 30 min in a tube furnace. A  $\text{TiO}_2$  coated  $\text{Ta}_3\text{N}_5$  electrode without calcination was also prepared as a reference.

### 2.3 Coating of a $\text{Ni}(\text{OH})_x/\text{FeOOH}$ bi-layer electrocatalyst

A FeOOH layer and a  $\text{Ni}(\text{OH})_x$  layer were deposited on a  $\text{TiO}_2$  coated  $\text{Ta}_3\text{N}_5$  photoelectrode by CBD method and electro-deposition method,<sup>24</sup> respectively. A FeOOH layer was deposited in a mixture of 50 mM  $\text{Fe}(\text{NO}_3)_3$  and 500 mM  $\text{NaNO}_3$  aqueous solution at 100 °C for 20 min. After washed with distilled water and dried in air, a  $\text{Ni}(\text{OH})_x$  layer was electro-

deposited with a potential of  $-0.85$  V *vs.* saturated calomel electrode (SCE) in 0.1 M  $\text{NiSO}_4$  aqueous solution at room temperature. The deposition charge was about 12 mC cm<sup>-2</sup>.

### 2.4 Characterization of samples

The crystal structures of samples were measured by X-ray diffraction patterns (XRD, Bruker D8 ADVANCE diffractometer). The morphologies of samples were observed by field-emission scanning electron microscopy (FE-SEM, Nova NanoSEM 230, FEI). XPS spectra of samples were obtained by using a Thermo ESCALAB 250 machine and the binding energy was calibrated by C1s (284.8 eV).

### 2.5 Photoelectrochemical measurement

The photoelectrochemical properties were conducted in an electrochemical analyzer (CHI-660D, Shanghai Chenhua). A  $\text{Ta}_3\text{N}_5$  electrode, SCE and Pt foil were used as the working electrode, reference electrode and counter electrode, respectively. 1 M NaOH (pH = 13.6) aqueous solution was used as electrolyte. A reversible hydrogen electrode (RHE) potential was obtained by the formula:

$$E(\text{V} \text{ vs. RHE}) = E(\text{V} \text{ vs. SCE}) + 0.242V + 0.059 \times \text{pH}$$

A Xe lamp and AM 1.5G sunlight simulator (100 mW cm<sup>-2</sup>, Newport oriel 92251A-1000) were used as light sources, respectively. The electrochemical impedance spectra (EIS) of samples were measured by an electrochemical analyzer (Solartron1260 + 1287) with a 10 mV amplitude perturbation and frequencies between 0.1 Hz and 10 MHz. The incident photon-to-current efficiency (IPCE) was measured under irradiation of different wavelengths of light generated by monochromatic filters. A photometer (Newport, 840-C, USA) was used to detect light intensity. The IPCE was calculated as follow:

$$\text{IPCE} = 1240 \times I_{\text{ph}}/P\lambda$$

where  $I_{\text{ph}}$  is photocurrent density ( $\mu\text{A cm}^{-2}$ ),  $P$  and  $\lambda$  are incident light intensity ( $\mu\text{W cm}^{-2}$ ) and wavelength (nm), respectively.

## 3. Results and discussion

### 3.1 Improved efficiency of $\text{Ta}_3\text{N}_5$ by etching a Ta foil precursor with HF solution

In our previous study, a smooth and thin layer of  $\text{Ta}_3\text{N}_5$  with high oxygen impurity existed on the surface of an as-prepared sample, which played a role as surface recombination center and lowered the conversion efficiency of  $\text{Ta}_3\text{N}_5$ . By removing the  $\text{Ta}_3\text{N}_5$  surface layer through thermal or mechanical exfoliation method, an efficient  $\text{Ta}_3\text{N}_5$  photoanode was obtained.<sup>14</sup> In this study, a new surface etching approach was carried out on a Ta foil precursor with HF aqueous solution before oxidation and nitridation. The oxidation temperature was 554 °C, lower than the critical temperature of 590 °C.<sup>14</sup> Therefore, no surface thermal exfoliation was observed on the  $\text{Ta}_3\text{N}_5$  samples in this study. Fig. 1a and b shows SEM images of  $\text{Ta}_3\text{N}_5$  from Ta foil



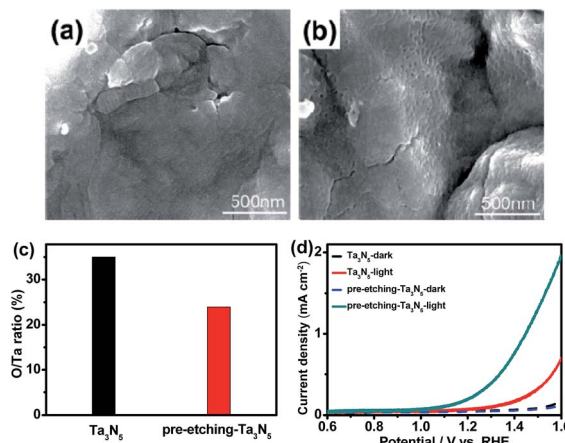


Fig. 1 SEM images of  $\text{Ta}_3\text{N}_5$  from Ta foil precursor without (a) and with (b) surface etching; (c) O/Ta ratios on the surface of  $\text{Ta}_3\text{N}_5$  by XPS from a Ta foil precursor with and without surface etching; (d) current–potential curves of  $\text{Ta}_3\text{N}_5$  photoanodes from Ta foil precursor with and without surface etching in 1 M NaOH aqueous solution ( $\text{pH} = 13.6$ ) under xenon lamp irradiation.

precursor without and with surface etching, respectively. Without surface etching, a smooth surface is observed on the sample. The surface becomes rougher after surface etching of Ta foil precursor and some particles, aggregates and grooves are observed. XRD (see Fig. S1a and Table S1†) and Raman (see Fig. S1b†) results suggest that there are no obvious differences in crystal structures and grain sizes between the two samples before and after etching. XPS indicates the ratio of O/Ta on the surface of  $\text{Ta}_3\text{N}_5$  decreases from 0.35 to 0.24 after surface etching of Ta foil precursor (see Fig. 1c). The surface etching of Ta foil precursor with HF solution is a new method to remove an oxygen-rich surface layer. Fig. 1d indicates photoelectrochemical properties of  $\text{Ta}_3\text{N}_5$  photoanodes from Ta foils with and without surface etching. After surface etching, the performance of a  $\text{Ta}_3\text{N}_5$  photoanode increases remarkably, which comes from the surface oxygen-rich layer removal. The result is in good agreement with our previous study.

### 3.2 Effect of post-heating a $\text{TiO}_2$ passivation layer on a photo-potential of a $\text{Ta}_3\text{N}_5$ photoanode

Efficient  $\text{Ni}(\text{OH})_x/\text{FeOOH}$  bilayer electrocatalysts for OER were coated on the surface of  $\text{Ta}_3\text{N}_5$  photoanodes to accelerate the water oxidation process, following a previous report.<sup>24</sup> In this study, a  $\text{Ni}(\text{OH})_x/\text{FeOOH}$  coated  $\text{Ta}_3\text{N}_5$  sample is referred as  $\text{Ta}_3\text{N}_5/\text{F/N}$ . In order to further decrease the surface recombination of  $\text{Ta}_3\text{N}_5$ , post-heating a  $\text{TiO}_2$  passivation layer in nitrogen atmosphere at different temperatures was carried out. Fig. 2a indicates photoelectrochemical properties of  $\text{Ta}_3\text{N}_5/\text{TiO}_2/\text{F/N}$  after post-heating  $\text{TiO}_2$  at different temperatures, and  $\text{Ta}_3\text{N}_5/\text{F/N}$  references without a  $\text{TiO}_2$  layer before and after calcining at 200 °C. After coating a  $\text{TiO}_2$  passivation layer, an onset potential of  $\text{Ta}_3\text{N}_5/\text{F/N}$  shifts cathodically, which is in good agreement with previous study.<sup>31</sup> However, in previous studies,<sup>24,31</sup> no post-treatment of a  $\text{TiO}_2$  passivation layer was

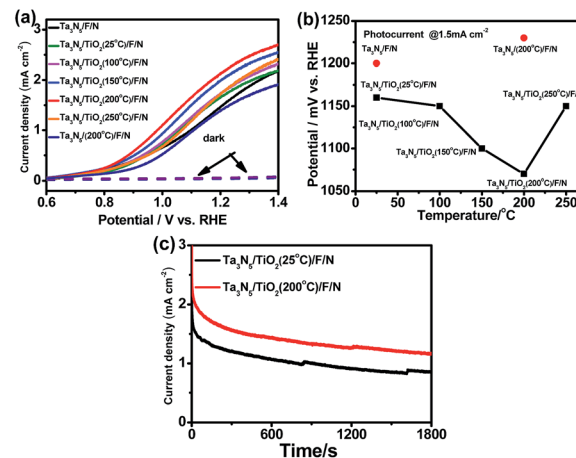


Fig. 2 (a) Current–potential curves of  $\text{Ta}_3\text{N}_5/\text{F/N}$ ,  $\text{Ta}_3\text{N}_5/\text{TiO}_2$  (25 °C)/F/N,  $\text{Ta}_3\text{N}_5/\text{TiO}_2$  (100 °C)/F/N,  $\text{Ta}_3\text{N}_5/\text{TiO}_2$  (150 °C)/F/N,  $\text{Ta}_3\text{N}_5/\text{TiO}_2$  (200 °C)/F/N,  $\text{Ta}_3\text{N}_5/\text{TiO}_2$  (250 °C)/F/N and  $\text{Ta}_3\text{N}_5$  (200 °C)/F/N without  $\text{TiO}_2$  in 1 M NaOH ( $\text{pH} = 13.6$ ) under 300 W xenon lamp irradiation; (b) photo-potentials @1.5  $\text{mA cm}^{-2}$  of the samples vs. post-heating temperatures; (c) current density–time curves of  $\text{Ta}_3\text{N}_5/\text{TiO}_2$  (25 °C)/F/N and  $\text{Ta}_3\text{N}_5/\text{TiO}_2$  (200 °C)/F/N at 1.23 V<sub>RHE</sub> under 300 W xenon lamp irradiation.

carried out to further improve the performance of a  $\text{Ta}_3\text{N}_5$  photoanode. In this study, after post-heating a  $\text{TiO}_2$  passivation layer in  $\text{N}_2$  at different temperatures for 30 min, the onset potential of  $\text{Ta}_3\text{N}_5/\text{F/N}$  with a  $\text{TiO}_2$  passivation layer is cathodically shifted. The optimized post-heating temperature is 200 °C. Compared to the sample post-heating at 200 °C, an onset potential of  $\text{Ta}_3\text{N}_5/\text{TiO}_2/\text{F/N}$  with post-heating at 250 °C is anodic shifted. An onset potential of  $\text{Ta}_3\text{N}_5/\text{F/N}$  without a  $\text{TiO}_2$  passivation layer is also anodic shifted after post-heating  $\text{Ta}_3\text{N}_5$  in  $\text{N}_2$  at 200 °C for the same time. The results suggest that the cathodic shift of onset potentials of  $\text{Ta}_3\text{N}_5/\text{F/N}$  with a  $\text{TiO}_2$  passivation layer after post-heating does not come from post-heating  $\text{Ta}_3\text{N}_5$ , but the  $\text{TiO}_2$  passivation layer.

Fig. 2b shows the photo-potential (@1.5  $\text{mA cm}^{-2}$ ) of the samples with post-heating  $\text{TiO}_2$  at different temperatures. After coating a  $\text{TiO}_2$  passivation layer at room temperature, a photo-potential of a  $\text{Ta}_3\text{N}_5/\text{F/N}$  is cathodically shifted about 40 mV. A photo-potential is further cathodically shifted about 10 mV, 60 mV and 90 mV after post-heating  $\text{TiO}_2$  passivation layers at 100 °C, 150 °C and 200 °C, respectively. Two kinds of slopes of photo-potential decrease are observed at the post-heating temperature lower and higher than 100 °C, suggesting 100 °C is a critical temperature to activate the  $\text{TiO}_2$  passivation layer. When the post-heating temperature is increased to 250 °C, a photo-potential is anodically shifted about 50 mV, which comes from decreased performance of a  $\text{Ta}_3\text{N}_5$  photoanode after post-heated at such a high temperature. The result suggests that the improved performance of a  $\text{TiO}_2$  coated  $\text{Ta}_3\text{N}_5$  comes from the post-heating treatment of  $\text{TiO}_2$  but not  $\text{Ta}_3\text{N}_5$ . Fig. 2c indicates the photo-stability of  $\text{Ta}_3\text{N}_5/\text{TiO}_2/\text{F/N}$  with and without post-heating  $\text{TiO}_2$  at 200 °C. Photo-stability of the two samples is similar and the increased photocurrent can be kept during 1800 s illumination, suggesting that the post-heating treatment makes  $\text{Ta}_3\text{N}_5/\text{TiO}_2/\text{F/N}$  change irreversibly.

### 3.3 A mechanism for improved performance of a $\text{Ta}_3\text{N}_5$ photoanode by post-heating a $\text{TiO}_2$ passivation layer

Fig. 3 indicates surface morphologies of  $\text{Ta}_3\text{N}_5$ ,  $\text{Ta}_3\text{N}_5/\text{TiO}_2$  (25 °C),  $\text{Ta}_3\text{N}_5/\text{TiO}_2$  (200 °C) and  $\text{Ta}_3\text{N}_5/\text{TiO}_2$  (200 °C)/F/N, respectively. Some pores are observed on the surface of  $\text{Ta}_3\text{N}_5$ , which comes from decreased quantity of anions after nitriding  $\text{Ta}_2\text{O}_5$  into  $\text{Ta}_3\text{N}_5$ .<sup>34</sup> No obvious morphology change is observed after coating and post-heating a  $\text{TiO}_2$  passivation layer at 200 °C, which suggests that the  $\text{TiO}_2$  layer is very thin (Fig. 3b and c), several nanometer, according to previous study.<sup>24</sup> After loading a  $\text{Ni(OH)}_x/\text{FeOOH}$  bilayer electrocatalyst, some nanoparticles uniformly distribute on the surface of a  $\text{Ta}_3\text{N}_5$  photoanode (see Fig. 3d). X-ray diffraction patterns (XRD) and Raman was also employed to characterize  $\text{TiO}_2$  on the surface of  $\text{Ta}_3\text{N}_5$  samples with post-heating  $\text{TiO}_2$  at different temperatures (see Fig. S3 and S4†). All the samples show the same XRD and Raman patterns with a bare  $\text{Ta}_3\text{N}_5$  sample and no  $\text{TiO}_2$ 's signal is observed possibly due to the thin and poor crystalline of a  $\text{TiO}_2$  layer.

Fig. 4a and b show XPS peaks of  $\text{Ta}4\text{f}$  and  $\text{N}1\text{s}$  in  $\text{TiO}_2$  coated  $\text{Ta}_3\text{N}_5$  samples at different post-heating temperatures, respectively. Binding energies of  $\text{Ta}4\text{f}$  (25.2 eV and 27.1 eV) in Fig. 4a are assigned to  $\text{Ta}^{5+}$  in a  $\text{TiO}_2$  coated  $\text{Ta}_3\text{N}_5$  without post-heating, which do not shift after post-heating at temperatures of 100 °C, 150 °C and 200 °C. However, the binding energies shift to lower values about 0.1 eV after post-heating at 250 °C. Fig. 4b indicates similar trend of  $\text{N}1\text{s}$  with that in Fig. 4a. The results suggest that the valence state of  $\text{Ta}^{5+}$  and  $\text{N}^{3-}$  in  $\text{Ta}_3\text{N}_5$  did not change when post-heating at a temperature lower than 200 °C. However,  $\text{Ta}_3\text{N}_5$  is oxidized during post-heating at 250 °C due to residual  $\text{O}_2$  impurity in  $\text{N}_2$  carrier gas.<sup>35,36</sup> The binding energies of  $\text{Ti}2\text{p}$  (465 eV and 459 eV) in Fig. 4c are assigned to  $\text{Ti}^{4+}$ ,<sup>37,38</sup> which shift to lower binding energy as post-heating temperatures increase. The peak shift possibly comes from dehydration of titanium hydroxides into  $\text{TiO}_x$  at high temperatures.<sup>38</sup>

Fig. 5a shows the XPS spectra of  $\text{O}1\text{s}$  in the  $\text{Ta}_3\text{N}_5/\text{TiO}_2$  at different post-heating temperatures. Three kinds of peaks

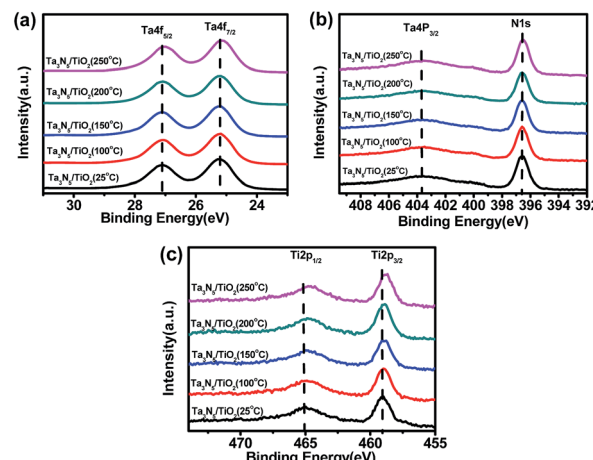


Fig. 4 XPS spectra of (a)  $\text{Ta}4\text{f}_{5/2}$  and  $\text{Ta}4\text{f}_{7/2}$ , (b)  $\text{Ta}4\text{p}_{3/2}$  and  $\text{N}1\text{s}$ , (c)  $\text{Ti}2\text{p}_{1/2}$  and  $\text{Ti}2\text{p}_{3/2}$  of  $\text{Ta}_3\text{N}_5/\text{TiO}_2$  (25 °C),  $\text{Ta}_3\text{N}_5/\text{TiO}_2$  (100 °C),  $\text{Ta}_3\text{N}_5/\text{TiO}_2$  (150 °C),  $\text{Ta}_3\text{N}_5/\text{TiO}_2$  (200 °C),  $\text{Ta}_3\text{N}_5/\text{TiO}_2$  (250 °C).

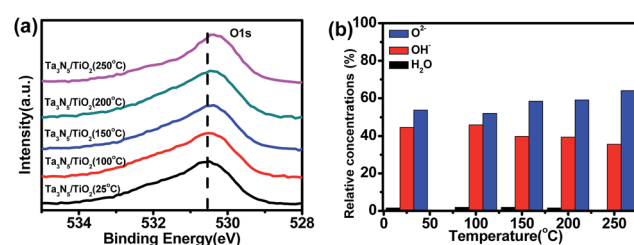


Fig. 5 (a) XPS spectra of  $\text{O}1\text{s}$  (b) relative concentrations of adsorbed  $\text{H}_2\text{O}$  (dark), lattice  $\text{OH}^-$  (red), lattice  $\text{O}^{2-}$  (blue) vs. post-heating temperatures and (c) ratio of  $\text{OH}^-$  to  $\text{O}^{2-}$  on the surface of  $\text{Ta}_3\text{N}_5/\text{TiO}_2$  (25 °C),  $\text{Ta}_3\text{N}_5/\text{TiO}_2$  (100 °C),  $\text{Ta}_3\text{N}_5/\text{TiO}_2$  (150 °C),  $\text{Ta}_3\text{N}_5/\text{TiO}_2$  (200 °C),  $\text{Ta}_3\text{N}_5/\text{TiO}_2$  (250 °C).

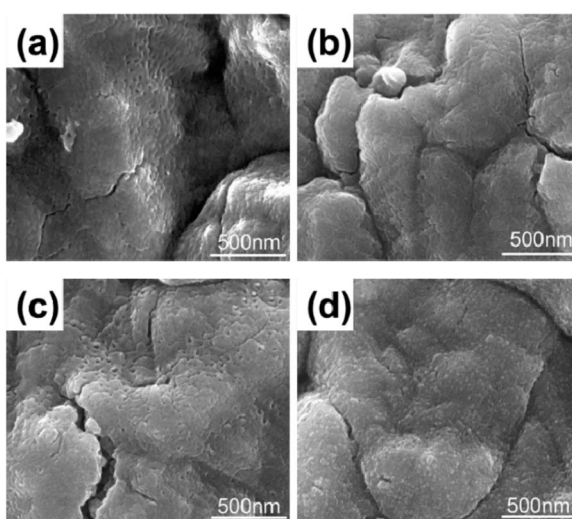


Fig. 3 Surface SEM images of (a)  $\text{Ta}_3\text{N}_5$ , (b)  $\text{Ta}_3\text{N}_5/\text{TiO}_2$  (25 °C), (c)  $\text{Ta}_3\text{N}_5/\text{TiO}_2$  (200 °C), (d)  $\text{Ta}_3\text{N}_5/\text{TiO}_2$  (200 °C)/F/N.

(530.4 eV, 531.5 eV and 533.5 eV) are used to fit XPS spectra of  $\text{O}1\text{s}$ , which are assigned to lattice  $\text{O}^{2-}$ , lattice  $\text{OH}^-$  and adsorbed  $\text{H}_2\text{O}$  (see Fig. S5†), respectively.<sup>39,40</sup> The relative concentrations of these three kinds of oxygen species are calculated from XPS data and the results are shown in Fig. 5b. The ratio of  $\text{OH}^-$  to  $\text{O}^{2-}$  in the sample without post-heating is 0.83, which does not change obviously after post-heating at 100 °C, and decreases to 0.55 when the calcination temperature is 250 °C (see Fig. 5c). The  $\text{OH}^-$  content of the samples decreases with higher post-heating temperature, due to the dehydration reaction during the post-heating process:<sup>41</sup>  $\text{Ti-OH} + \text{HO-Ti} \rightarrow \text{Ti-O-Ti} + \text{H}_2\text{O}$ . Therefore, the post-heating of a  $\text{TiO}_2$  coated  $\text{Ta}_3\text{N}_5$  leads to a reduction of  $\text{OH}^-$  content in the  $\text{TiO}_2$  passivation layer. However, when the post-heating temperature is lower than



100 °C, no  $\text{OH}^-$  decrease is observed. These results suggest that there is a barrier for the dehydration reaction.

In order to understand the effect of post-heating on photo-potential of a  $\text{TiO}_2$  coated  $\text{Ta}_3\text{N}_5$ , electrochemical impedance spectroscopy (EIS) measurement of the samples was also carried out and the results are shown in Fig. 6a. An equivalent circuit is plotted in the inset of Fig. 6a.  $R_{\text{ct}}$ ,  $R_{\text{s}}$ , and CPE represent a charge transfer resistance in semiconductor-electrolyte interface, an electrolyte resistance and a constant phase element of a double layer, respectively.<sup>31</sup> The semicircle of a  $\text{TiO}_2$  coated  $\text{Ta}_3\text{N}_5$  with post-heating at 200 °C is the smallest, indicating a fastest interface charge transfer speed among the five samples. Fig. 6b shows the  $R_{\text{ct}}$  values of the  $\text{TiO}_2$  coated  $\text{Ta}_3\text{N}_5$  samples with post-heating at different temperatures. There is a positive correlation between the performance of a  $\text{TiO}_2$  coated  $\text{Ta}_3\text{N}_5$  and interface charge transfer. Therefore, reduced  $\text{OH}^-$  content in the  $\text{TiO}_2$  passivation layer after the post-heating process, which leads to an increase of interface charge transfer and cathodic shift of the photo-potential.

Photocurrent-potential curves of  $\text{Ta}_3\text{N}_5$  before and after depositing  $\text{TiO}_2$  layer in 1 M NaOH with  $\text{H}_2\text{O}_2$  as sacrificial reagent were measured and the results are shown in Fig. S6a.<sup>†</sup> From Fig. S6a,<sup>†</sup> the photocurrent of  $\text{Ta}_3\text{N}_5$  in the solution with sacrificial reagent are similar to the samples after depositing a  $\text{TiO}_2$  layer and post-heating  $\text{TiO}_2$  layer, which suggests that charge separation efficiency does not change after depositing the  $\text{TiO}_2$  layer.<sup>15</sup> Therefore, the improved performance of a  $\text{TiO}_2$  coated  $\text{Ta}_3\text{N}_5$  photoanode for water oxidation comes from enhanced interfacial charge transfer efficiency, which is in agreement with previous study.<sup>24</sup> Both loading oxygen evolution reaction (OER) catalysts and passivating surface defect states by noncatalysts can enhance interfacial charge transfer efficiency.<sup>42</sup> In order to investigate the role of a  $\text{TiO}_2$  layer, current-potential curves of FTO, FTO/ $\text{TiO}_2$  and FTO/ $\text{TiO}_2$  (200 °C) for oxygen evolution reaction are shown in Fig. S6b.<sup>†</sup> The OER current of FTO decreases after depositing a  $\text{TiO}_2$  layer, whether post-heating or not. The results suggest that no catalysis effects are observed on the  $\text{TiO}_2$  layer, which are in good agreement with previous studies.<sup>24,32,33</sup> Therefore, the  $\text{TiO}_2$  layer plays a role as a passivation layer,<sup>31,43</sup> which reduces the surface carrier recombination and facilitate interfacial charge transfer.

According to XPS and EIS results, a mechanism of cathodic shift photo-potential after post-heating a  $\text{TiO}_2$  layer is illustrated in Fig. 7. Before post-heating, holes are generated in the

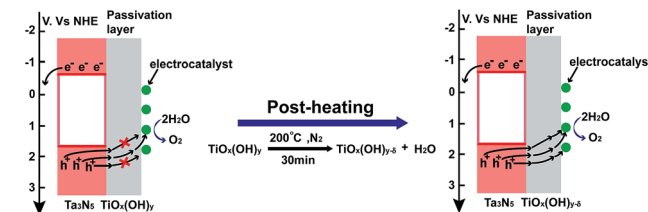


Fig. 7 Illustration of energy band positions and interface charge transfer in a  $\text{TiO}_2$  coated  $\text{Ta}_3\text{N}_5$  before and after post-heating.

valence band of  $\text{Ta}_3\text{N}_5$ , which transfer to the  $\text{TiO}_2$  passivation layer and then to electrocatalysts for water oxidation under illumination. From EIS in Fig. 6, large amount of  $\text{OH}^-$  in the as-deposited  $\text{TiO}_2$  decreases conductivity of  $\text{TiO}_2$  and limits hole transfer in the  $\text{TiO}_2$  passivation layer. After post-heating,  $\text{OH}^-$  content in  $\text{TiO}_2$  decrease and increase the conductivity of the passivation layer. Therefore, hole transfer in a  $\text{TiO}_2$  passivation layer is increased after post-heating. However, if the post-heating temperature is too high (250 °C),  $\text{Ta}_3\text{N}_5$  can be oxidized and the performance of the samples becomes lower. Therefore, an optimum post-heating temperature is observed.

### 3.4 Performance of a $\text{Ta}_3\text{N}_5$ photoanode with post-heating a $\text{TiO}_2$ passivation layer under sunlight simulator illumination

Fig. 8a shows current-potential curves of the  $\text{Ta}_3\text{N}_5/\text{TiO}_2$  (200 °C)/F/N under a standard measurement condition to compare the performance of our sample with previous studies. A photocurrent of  $6.4 \text{ mA cm}^{-2}$  at  $1.23 \text{ V}_{\text{RHE}}$  is achieved in the  $\text{Ta}_3\text{N}_5/\text{TiO}_2$  (200 °C)/F/N. The IPCEs at  $1.23 \text{ V}_{\text{RHE}}$  of the samples were measured and the results are shown in Fig. 8b. An integrated photocurrent is calculated as  $6.2 \text{ mA cm}^{-2}$  from IPCEs at the standard solar spectrum, which is consistent with the measured value in Fig. 8a. Therefore, the solar photocurrent in

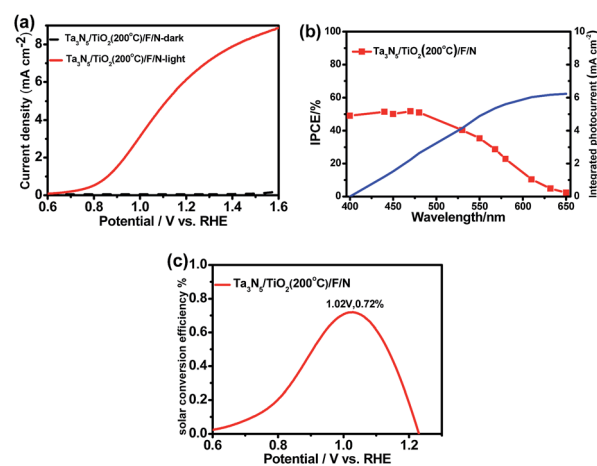


Fig. 8 (a) A current-potential curve of  $\text{Ta}_3\text{N}_5/\text{TiO}_2$  (200 °C)/F/N photoanode and (b) the corresponding IPCEs at  $1.23 \text{ V}_{\text{RHE}}$ ; (c) a half-cell solar to hydrogen efficiency electrolyte: 1 M NaOH (pH = 13.6), light source: AM 1.5G simulated sunlight ( $100 \text{ mW cm}^{-2}$ ).

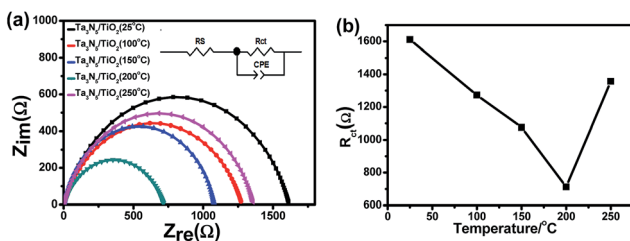


Fig. 6 (a) EIS of  $\text{Ta}_3\text{N}_5/\text{TiO}_2$  (25 °C),  $\text{Ta}_3\text{N}_5/\text{TiO}_2$  (100 °C),  $\text{Ta}_3\text{N}_5/\text{TiO}_2$  (150 °C),  $\text{Ta}_3\text{N}_5/\text{TiO}_2$  (200 °C),  $\text{Ta}_3\text{N}_5/\text{TiO}_2$  (250 °C); (b) interface charge transfer resistance  $R_{\text{ct}}$  vs. post-heating temperatures.



Fig. 8a is reliable. A half-cell solar to hydrogen efficiency (HC-*STH*) is calculated as 0.72% at 1.02 V<sub>RHE</sub> (Fig. 8c). The photocurrent at 1.23 V<sub>RHE</sub> and HC-*STH* are the highest values among Ta<sub>3</sub>N<sub>5</sub> photoanodes prepared by oxidation and nitridation of Ta foils method. The results suggest that post-heating is an effective strategy to obtain efficient TiO<sub>2</sub> coated Ta<sub>3</sub>N<sub>5</sub> photoanodes for solar water splitting.

## 4. Conclusion

In summary, a new etching method was used to remove an oxygen-rich surface layer of Ta<sub>3</sub>N<sub>5</sub> and enhanced the performance of a Ta<sub>3</sub>N<sub>5</sub> photoanode. The conversion efficiency of Ta<sub>3</sub>N<sub>5</sub> was improved by coating a TiO<sub>2</sub> passivation layer on the surface. We found that amount of OH<sup>-</sup> decreased the conductivity of an as-deposited TiO<sub>2</sub> layer, which limited the performance of a TiO<sub>2</sub> coated Ta<sub>3</sub>N<sub>5</sub>. Therefore, a post-heating treatment was proposed to decrease OH<sup>-</sup> species and increase the conductivity of TiO<sub>2</sub>, which cathodically shifted the photo-potential of Ta<sub>3</sub>N<sub>5</sub> about 90 mV. After the post-heating, a photocurrent of 6.4 mA cm<sup>-2</sup> at 1.23 V<sub>RHE</sub> and a HC-*STH* efficiency of 0.72% were obtained in a TiO<sub>2</sub> coated Ta<sub>3</sub>N<sub>5</sub> photoanode with Ni(OH)<sub>x</sub>/FeOOH bilayer electrocatalyst, which are the highest values among Ta<sub>3</sub>N<sub>5</sub> photoanodes prepared by thermal oxidation and nitridation of Ta foils.

## Acknowledgements

This work is financially supported by the National Basic Research Program of China (973 Program, No. 2015CB932200, 2014CB239303 and 2013CB632404), the Natural Science Foundation of Jiangsu Province of China (No. 15KJB150010 and No. BK20150955), Synergetic Innovation Center for Organic Electronics and Information Displays, the Priority Academic Program Development of Jiangsu Higher Education Institutions (PAPD). Wenjun Luo and Wei Huang acknowledge a Newton Research Collaboration Programme Type 2 Award (No. NRCP/1415/264).

## Notes and references

- 1 A. Fujishima and K. Honda, *Nature*, 1972, **238**, 37–38.
- 2 M. Gratzel, *Nature*, 2001, **414**, 338–344.
- 3 M. G. Walter, E. L. Warren, J. R. McKone, S. W. Boettcher, Q. Mi, E. A. Santori and N. S. Lewis, *Chem. Rev.*, 2010, **110**, 6446–6473.
- 4 O. Khaselev, A. Bansal and J. A. Turner, *Int. J. Hydrogen Energy*, 2001, **26**, 127–132.
- 5 M. C. Hanna and A. J. Nozik, *J. Appl. Phys.*, 2006, **100**, 074510.
- 6 O. Khaselev and J. A. Turner, *Science*, 1998, **280**, 425–427.
- 7 K. Ohashi, J. McCann and J. O. M. Bockris, *Nature*, 1977, **266**, 610–611.
- 8 J. Akikusa and S. U. M. Khan, *Int. J. Hydrogen Energy*, 2002, **27**, 863–870.
- 9 A. J. Nozik, *Appl. Phys. Lett.*, 1976, **29**, 150–153.
- 10 L. Fornarini, A. J. Nozik and B. A. Parkinson, *J. Phys. Chem.*, 1984, **88**, 3238–3243.
- 11 M. S. Prévot and K. Sivula, *J. Phys. Chem. C*, 2013, **117**, 17879–17893.
- 12 W. Luo, Z. Yang, Z. Li, J. Zhang, J. Liu, Z. Zhao, Z. Wang, S. Yan, T. Yu and Z. Zou, *Energy Environ. Sci.*, 2011, **4**, 4046–4051.
- 13 D. P. Cao, W. J. Luo, J. Y. Feng, X. Zhao, Z. S. Li and Z. G. Zou, *Energy Environ. Sci.*, 2014, **7**, 752–759.
- 14 M. Li, W. Luo, D. Cao, X. Zhao, Z. Li, T. Yu and Z. Zou, *Angew. Chem., Int. Ed.*, 2013, **52**, 11016–11020.
- 15 Z. Li, W. Luo, M. Zhang, J. Feng and Z. Zou, *Energy Environ. Sci.*, 2013, **6**, 347–370.
- 16 S. D. Tilley, M. Cornuz, K. Sivula and M. Graetzel, *Angew. Chem., Int. Ed.*, 2010, **49**, 6405–6408.
- 17 S. C. Warren, K. Voitchovsky, H. Dotan, C. M. Leroy, M. Cornuz, F. Stellacci, C. Hebert, A. Rothschild and M. Graetzel, *Nat. Mater.*, 2013, **12**, 842–849.
- 18 M. N. Huda, A. Walsh, Y. Yan, S.-H. Wei and M. M. Al-Jassim, *J. Appl. Phys.*, 2010, **107**, 123712.
- 19 G. Hitoki, A. Ishikawa, T. Takata, J. N. Kondo, M. Hara and K. Domen, *Chem. Lett.*, 2002, **7**, 736–737.
- 20 C. M. Fang, E. Orhan, G. A. de Wijs, H. T. Hintzen, R. A. de Groot, R. Marchand, J. Y. Saillard and G. de With, *J. Mater. Chem.*, 2001, **11**, 1248–1252.
- 21 W. J. Chun, A. Ishikawa, H. Fujisawa, T. Takata, J. N. Kondo, M. Hara, M. Kawai, Y. Matsumoto and K. Domen, *J. Phys. Chem. B*, 2003, **107**, 1798–1803.
- 22 Y. Li, L. Zhang, A. Torres-Pardo, J. M. Gonzalez-Calbet, Y. Ma, P. Oleynikov, O. Terasaki, S. Asahina, M. Shima, D. Cha, L. Zhao, K. Takanabe, J. Kubota and K. Domen, *Nat. Commun.*, 2013, **4**, 2566.
- 23 L. Wang, X. Zhou, N. T. Nguyen, I. Hwang and P. Schmuki, *Adv. Mater.*, 2016, **28**, 2432–2438.
- 24 G. Liu, S. Ye, P. Yan, F. Xiong, P. Fu, Z. Wang, Z. Chen, J. Shi and C. Li, *Energy Environ. Sci.*, 2016, **9**, 1327–1334.
- 25 M. Liao, J. Feng, W. Luo, Z. Wang, J. Zhang, Z. Li, T. Yu and Z. Zou, *Adv. Funct. Mater.*, 2012, **22**, 3066–3074.
- 26 G. Liu, J. Shi, F. Zhang, Z. Chen, J. Han, C. Ding, S. Chen, Z. Wang, H. Han and C. Li, *Angew. Chem., Int. Ed.*, 2014, **53**, 7295–7299.
- 27 L. Wang, F. Dionigi, N. Nhat Truong, R. Kirchgeorg, M. Gliech, S. Grigorescu, P. Strasser and P. Schmuki, *Chem. Mater.*, 2015, **27**, 2360–2366.
- 28 C. Wang, T. Hisatomi, T. Minegishi, M. Nakabayashi, N. Shibata, M. Katayama and K. Domen, *J. Mater. Chem. A*, 2016, **4**, 13837–13843.
- 29 E. Nurlaela, S. Ould-Chikh, M. Harb, S. del Gobbo, M. Aouine, E. Puzenat, P. Sautet, K. Domen, J.-M. Bassat and K. Takanabe, *Chem. Mater.*, 2014, **26**, 4812–4825.
- 30 S. Hu, M. R. Shaner, J. A. Beardslee, M. Licherman, B. S. Brunschwig and N. S. Lewis, *Science*, 2014, **344**, 1005–1009.
- 31 P. Zhang, T. Wang and J. Gong, *Chem. Commun.*, 2016, **52**, 8806–8809.
- 32 X. Yang, R. Liu, C. Du, P. Dai, Z. Zheng and D. Wang, *ACS Appl. Mater. Interfaces*, 2014, **6**, 12005–12011.



33 M. G. Ahmed, I. E. Kretschmer, T. A. Kaniel, A. Y. Ahmed, F. A. Rashwan and D. W. Bahnemann, *ACS Appl. Mater. Interfaces*, 2015, **7**, 24053–24062.

34 B. A. Pinaud, P. C. K. Vesborg and T. F. Jaramillo, *J. Phys. Chem. C*, 2012, **116**, 15918–15924.

35 A. Ishikawa, T. Takata, J. N. Kondo, M. Hara and K. Domen, *J. Phys. Chem. B*, 2004, **108**, 11049–11053.

36 D. Yokoyama, H. Hashiguchi, K. Maeda, T. Minegishi, T. Takata, R. Abe, J. Kubota and K. Domen, *Thin Solid Films*, 2011, **519**, 2087–2092.

37 J. Yao, H. Shao, H. He and Z. Fan, *Appl. Surf. Sci.*, 2007, **253**, 8911–8914.

38 K. H. Wong, C. W. Mason, S. Devaraj, J. Ouyang and P. Balaya, *ACS Appl. Mater. Interfaces*, 2014, **6**, 2679–2685.

39 H. Perron, J. Vandeborre, C. Domain, R. Drot, J. Roques, E. Simoni, J. J. Ehrhardt and H. Catalette, *Surf. Sci.*, 2007, **601**, 518–527.

40 N. Kruse and S. Chenakin, *Appl. Catal., A*, 2011, **391**, 367–376.

41 J. G. Yu, H. G. Yu, B. Cheng, X. J. Zhao, J. C. Yu and W. K. Ho, *J. Phys. Chem. B*, 2003, **107**, 13871–13879.

42 R. Liu, Z. Zheng, J. Spurgeon and X. Yang, *Energy Environ. Sci.*, 2014, **7**, 2504–2517.

43 X. Li, P. S. Bassi, P. P. Boix, Y. Fang and L. H. Wong, *ACS Appl. Mater. Interfaces*, 2015, **7**, 16960–16966.

